Electron Spin Resonance of P Donors in Isotopically Purified Si Detected by Contactless Photoconductivity

Philipp Ross,[1] Brendon C. Rose,[2] Cheuk C. Lo,[1,3] Mike L.W. Thewalt,[4] Alexei M. Tyryshkin,[2] Stephen A. Lyon,[2] and John J.L. Morton[1,3,*]

[1] *London Centre for Nanotechnology, 17-19 Gordon Street, London WC1H 0AH, UK*

[2] *Department of Electrical Engineering, Princeton University, Princeton, New Jersey 08544, USA*

[3] *Department of Electronic and Electrical Engineering, University College London, Torrington Place, London WC1E 7JE, UK*

[4] *Simon Fraser University, Burnaby, British Columbia V5A 1S6, Canada*

(Received 5 February 2019; published 6 May 2019)

Coherence times of electron spins bound to phosphorus donors have been measured, using a standard Hahn echo technique, to be up to 20 ms in isotopically pure silicon with $[P] = 10^{14}$ cm^{-3} and at temperatures ≤ 4 K. Although such times are exceptionally long for electron spins in the solid state, they are nevertheless limited by donor electron spin-spin interactions. Suppressing such interactions requires even lower donor concentrations, which lie below the detection limit for typical ESR spectrometers. Here we describe an alternative method for phosphorus donor ESR detection, exploiting the spin-to-charge conversion provided by the optical donor-bound-exciton transition. We characterize the method and its dependence on laser power and use it to measure a coherence time of $T_2 = 130$ ms for one of the purest silicon samples grown to date ($[P] = 5 \times 10^{11}$ cm^{-3}). We then benchmark this result using an alternative application of the donor-bound-exciton transition: optically polarizing the donor spins before using conventional ESR detection at 1.7 K for a sample with $[P] = 4 \times 10^{12}$ cm^{-3}, and measuring in this case a T_2 of 350 ms. In both cases, T_2 is obtained after accounting for the effects of magnetic field noise, and the use of more stable (e.g., permanent) magnets could yield even longer coherence times.

DOI: 10.1103/PhysRevApplied.11.054014

I. INTRODUCTION

A number of factors are critical in the measurement of long coherence times in solid-state spin systems, including instrumental challenges such as stability in the magnetic field and microwave phase, as well as host crystal purity. In the case of silicon, isotopically enriched ^{28}Si crystals [1] have been used to extend the coherence time limits of both nuclear and electron donor spins in bulk samples [2–5], as well as in nanoscale single-donor devices [6]. However, while purifying the host environment is important, spin-spin interactions between same-species donors also play a limiting factor, due to the finite donor concentration within the sample. For example, from a ^{28}Si sample with $[P] = 10^{14}$ cm^{-3}, a coherence time of up to approximately 20 ms was measured [4], and shown to be limited by dipolar interactions between phosphorus donor spins. These interactions cannot be reversed in a standard Hahn echo measurement (this effect is also known as "instantaneous diffusion" [7,8]), however, their effect can be reduced by artificially reducing the spin concentration of the sample using a spin-echo sequence with shortened refocussing pulse. Such methods enable an estimate for the expected coherence times in more dilute samples, and led to inferred decay times of approximately 1 s [4]. However, the method does not account for other effects, which may be present in samples with low donor concentrations, such as donor-acceptor recombination.

Conventional ESR spectrometers are close to their detection limits for spin concentrations in the range of 10^{12} cm^{-3} and above, and thus new detection methods are needed in order to directly measure spin donor concentration times in samples with lower doping densities. Electrically detected magnetic resonance (EDMR) has been shown as a technique to study small numbers of donor electron spins [9] down to the level of 100 donors [10], however, most experiments have relied on coupling to spin-active defects at the $Si - SiO_2$ interface for readout, and in such cases T_2 is typically of order 1 μs [11]. EDMR methods have recently been combined with the use of donor-bound-exciton D^0X spectroscopy to measure intrinsic donor spin coherence times [12], leading to a maximum T_2 of about 1.5 ms, in that case still limited by the donor concentration.

*jjl.morton@ucl.ac.uk

In this paper, we report the coherence time measurement of two ^{28}Si samples with [P] $= 5 \times 10^{11}$ cm^{-3} and 4×10^{12} cm^{-3}, using spin-selective ionization via the donor-bound-exciton transition D^0X to optically polarize the spin ensemble beyond the thermal equilibrium value [12,13]. We then perform either a conventional ESR experiment (for the higher concentration sample) or measure the donor electron spin state via the spin-dependent photoconductivity following D^0X excitation [2,12,14], using a contactless technique where the sample is inserted into a parallel-plate capacitor. We fully characterize this contactless measurement method, studying the on- and off-resonance conductivity of the sample as a function of laser power. We perform Hahn echo coherence time measurements and find a coherence time of $T_2 = 130$ ms for the lower doped sample [using full (π) refocussing pulses] at 4.5 K. We compare this time with that measured from the higher doped sample using hyperpolarized ESR, where we find a T_2 of 350 ms. To our knowledge, these are the longest coherence times reported to date for an electron spin in a solid state away from a clock transition [15], and using full refocussing pulses [4].

II. CONTACTLESS PHOTOCONDUCTIVE D^0X DETECTION

The basis for the hyperpolarization and the spin-to-charge conversion used here is the donor-bound-exciton transition. Neutral donors in silicon can be optically excited to the bound-exciton (D^0X) state in which two electrons and a hole bind to the donor. In the (D^0X) ground state the two electrons form a spin singlet and the hole spin ($J = 3/2$) determines the Zeeman splitting in an external magnetic field, as depicted in Fig. 1(c). The long bound-exciton lifetime (272 ns [16]) and relatively small inhomogeneous broadening result in D^0X optical transitions that are sufficiently narrow to enable the excitation of the donor selectively on its electron spin state [12] (and in low-strain ^{28}Si, even the donor nuclear spin state can be resolved [2,3]). The D^0X recombines via an Auger process, ejecting an electron into the conduction band and leaving behind the ionized donor, producing a change in sample conductivity.

We capacitively measure the conductivity change on D^0X resonance using the setup shown in Fig. 1(a): the silicon crystal ($2 \times 2 \times 10$ mm^3) is mounted between two printed circuit boards (PCBs) separated by two teflon spacers to minimize any applied stress to the sample, all placed within a quartz tube of 5 mm diameter. The copper electrodes of the PCB face outward to avoid direct electrical contact with the sample and are contacted via two cryogenic stainless steel coaxial cables. The probe stick is inserted into a dielectric ring microwave resonator and cooled to 4.5 K. We measure the capacitance C and loss tangent $D = \mathrm{Re}(Z)/|\mathrm{Im}(Z)|$ of the sample capacitor with

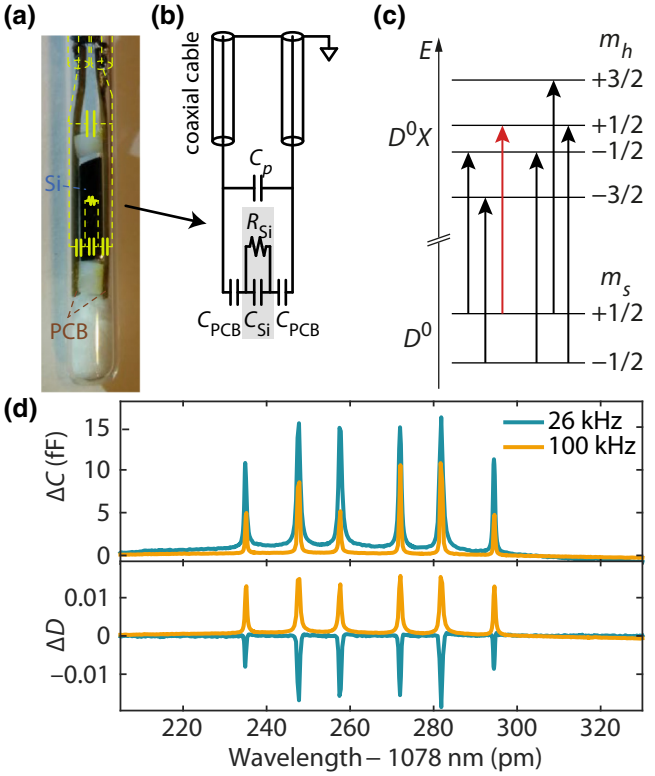

FIG. 1. The experimental setup and D^0X spectrum measured using contactless photoconductivity readout. (a) Photograph of the bottom of the probe stick and (b) its corresponding circuit diagram. (c) The six allowed D^0X transitions in a magnetic field, sorted by transition energy. The transition highlighted in red is used for ESR detection. (d) Changes of the capacitance C and loss tangent D for a ^{28}Si : P ([P] $= 2 \times 10^{14}$ cm^{-3}) in a magnetic field of 340 mT and a laser intensity of about 40 μW/mm^2.

an Agilent E4980D LCR meter ($V_{ac} = 1$ V, $V_{dc} = 0$ V, no resulting avalanche carrier generation), at some modulation frequency, f_m, and excite the D^0X transition using a NKT Boostik fibre laser with a nominal linewidth of 70 kHz.

Figure 1(d) shows a typical D^0X spectrum under an applied magnetic field. The six dipole-allowed D^0X transitions are observable both as a change in capacitance and as a change of the loss tangent D. We find that depending on the modulation frequency, we either observe an increase or decrease of the loss tangent on resonance, and explore this behavior in more detail. Figure 2 plots the capacitance and loss tangent of the sample as a function of modulaton frequency at $B = 0$ mT, both on and off resonance with the D^0X transition and for multiple different laser powers. We observe a steplike transition from a higher to a lower capacitance value with increasing frequency, coinciding with a peak in the loss tangent. This is a clear indication of a resonant phenomenon and we term this resonant frequency the "switching frequency," f_s in the following discussion. Increasing the applied laser power and

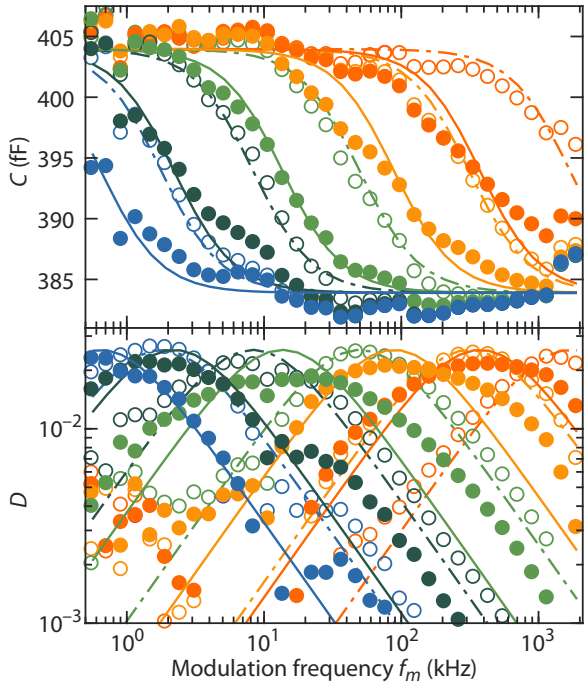

FIG. 2. Total capacitance, C, and loss tangent, D measured as a function of probe frequency and laser power, both on resonance (empty circles) and off resonance (filled circles) with the D^0X transition at $B = 0$ T. The laser power increases (nonlineary, see data points of Fig. 3) from 0.14 μW/mm^2 (blue) to 3.5 mW/mm^2 (red). [P] $= 3 \times 10^{15}$ cm^{-3}.

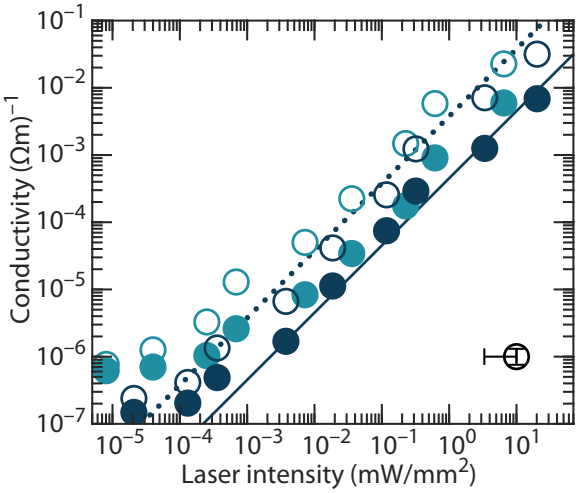

FIG. 3. Conductivity of the ^{28}Si : P with 2×10^{14} cm^{-3} (light blue) and 3×10^{15} cm^{-3} (dark blue) donors as a function of incident laser power, both on (open dots) and off (filled dots) resonance. The depicted typical error bar (bottom right) indicates the systematic error in delivered laser power due to the unknown absorption of cryostat and resonator windows and the statistical error of the conductivity fit.

bringing the laser on resonance with the D^0X transition are both characterized by an increase in f_s. These observations explain the modulation frequency-dependent behavior of the D^0X spectrum shown in Fig. 1(d), i.e., that C always increases on resonance with the D^0X transition, while D either increases or decreases depending on whether the modulation frequency is larger or smaller than f_s.

The underlying origin of the observed resonant behavior can be traced back to a change of sample conductivity with laser power. We employ the circuit model shown in Fig. 1(b) with the silicon sample modeled as a parallel circuit of some resistance R_{Si} and capacitance C_{Si}, sandwiched between two PCBs (of capacitance C_{PCB}) and a parasitic capacitance C_p in parallel. Under this model, we expect a larger measured capacitance for lower modulation frequencies because R_{Si} shorts the reactance associated with C_{Si} and thus the total capacitance is determined by the series connection of two C_{PCB}. As the frequency increases, the reactance associated with C_{Si} becomes smaller, until the capacitive reactance dominates the sample impedance. Thus, for higher frequencies the total capacitance is lower since it is the series capacitance of two C_{PCB} and C_{Si}. This transition occurs when the resistance R_{Si} and reactance $X_{\mathrm{Si}} = 1/(\omega C_{\mathrm{Si}})$ are equal, leading to the switching-frequency condition $f_s = \sigma_{\mathrm{Si}}/(2\pi\varepsilon_0\varepsilon_{\mathrm{r}})$, where σ_{Si} is the sample conductivity and $\varepsilon_{\mathrm{r}} = 11.45$ is the dielectric constant for Si at 4.5 K [17,18]. Using this circuit model we can fit the whole data set [both $C(\omega)$ and $D(\omega)$ simultaneously] reasonably well with a single value for $C_p = 290$ fF and $C_{\mathrm{PCB}} = 220$ fF. These values fit the expected parallel-plate capacitance by geometric considerations and secondly predict and match well the measured reduction of probe-stick capacitance after sample removal.

In Fig. 3, we plot the extracted sample conductivity σ_{Si} against laser power for two samples with different P concentrations, both on resonance with the D^0X transition (open dots) and off resonance (filled dots). We find a linear relationship between conductivity and laser power over 5 orders of magnitude, for both samples. The saturation of conductivity for laser powers smaller than 0.1 μW/mm^2 is likely due to background radiation leaking through the cryostat window. The conductivity is consistently larger by 5–8 times under on-resonant illumination compared to off-resonant illumination.

We first discuss the origin of conductivity when illuminating on resonance with the D^0X transition. Using the known oscillator strength [19] and the measured inhomogenous linewidth (1 GHz at 0 mT) of the D^0X transition we can estimate the steady-state D^0X carrier generation rate $G_{\mathrm{D^0X}}$, which is linearly dependent on the laser intensity I_L (see Appendix). The steady-state photocarrier density is then given by $n = G_{\mathrm{D^0X}}\tau_n$, where τ_n is the carrier lifetime, such that the conductivity under illumination is $\sigma = e\mu_n n = eG_{\mathrm{D^0X}}\mu_n\tau_n$. From the linear dependence of conductivity with laser power, we thus deduce that both

τ_n and μ_n are approximately constant for the laser intensities studied here. Furthermore, taking a silicon mobility of $\mu_n \sim 7 \times 10^4$ cm^2(Vs)$^{-1}$ appropriate at this temperature for these donor and acceptor concentrations [20], the slope in Fig. 3 (dotted line) can be fit to give $\tau_n \approx$ 7 ns. The photocarrier lifetime is expected to be limited by a capture process of the conduction-band electron by an ionized donor. The constant value of the carrier lifetime, which we observe, can be understood by considering the significant boron concentration in this material (in the region of 10^{14} cm^{-3}), which results in a substantial ionized donor concentration, even in the absence of any illumination. Indeed, the carrier concentration n is estimated to be 5×10^{10} cm^{-3} for $I_L = 10$ mW/mm^2 (see Appendix), such that the optically induced ionized donor concentration is negligible compared to that arising from the compensation in the material. Using the capture recombination coefficient [21,22] $B_{N^+} = 6.9 \times 10^{-6}$ cm^3 s^{-1}, we infer a constant ionized donor concentration of $N^+ = 2 \times 10^{13}$ cm^{-3} during illumination (see Appendix), consistent with the sample boron concentration [23].

The origin of the enhanced sample conductivity under off-resonant laser illumination is most likely the direct ionization of donors into the continuum of the conduction band, creating high-energy (hot) electrons. The ionization cross section for this process [22] is on the order of $\sigma_{N^0 \to N^+} \approx 10^{-16}$ cm^2, which would result in the solid blue line shown in Fig. 3 (following similar arguments to those given above and using the same $\tau_n \approx 7$ ns). In this way, both the on-resonant and off-resonant signal can be explained using known values for the generation rate and a common photocarrier lifetime. For completeness, a second mechanism that could produce similar observed behavior is phonon-assisted excitation across the bandgap. The photon energy at 1078 nm is below the silicon bandgap [24], requiring the absorption of a phonon for such across-gap excitation. However, at low temperatures the phonon bath is frozen out, leading to very small absorption coefficients below the bandgap [25,26].

The ratio of on- to off-resonant conductivity is between 5–8 for both donor concentrations studied here. This ratio is given by the relative magnitude of the D^0X generation rate versus the direct ionization rate of a donor. An outstanding question is the fact that the photoconductivity and laser intensity dependence we measure for two samples [P] $= 2 \times 10^{14}$ cm^{-3} and 3×10^{15} cm^{-3} are similar (see Fig. 3). The lower carrier generation rate expected for the sample with lower donor concentration may be somewhat compensated by a larger mobility and longer carrier lifetime, and may also be influenced by relatively small differences in the boron concentration (and thus ionized donor concentration) for which precise values are not known in these samples. A further study with a wider range of samples would be required to explore this in more detail.

III. COHERENCE TIME

Having characterized the change in sample conductivity upon excitation of the D^0X transition, we now use this as a readout mechanism to measure electron spin coherence times in ^{28}Si material with donor concentration below the sensitivity limits of conventional ESR. ([P] $= 5 \times 10^{11}$ cm^{-3}, [B] $= 10^{13}$ cm^{-3}.) We used a sequence of microwave (X-band, 9.75 GHz) and laser pulses, shown in Fig. 4(a), with the laser tuned to the $m_s = +1/2 : m_h = +1/2$ D^0X transition (see Fig. 1), addressing the spin $|\uparrow\rangle$ ground state, and a magnetic field of around 347 mT. Through optical pumping, the first laser pulse of 400 ms therefore polarizes and initializes the donor electron into the spin $|\downarrow\rangle$ state. A microwave Hahn echo pulse sequence follows, with a $(+/-)\pi/2$ pulse applied at the time of the electron spin-echo formation to project the refocused coherent electron spin state into $|\uparrow\rangle$ or $|\downarrow\rangle$, respectively. The final "readout" laser pulse creates a transient conductivity signal, which depends on the $|\uparrow\rangle$ population remaining at the end of the microwave pulse sequence. The time-resolved sample conductivity is measured using a lock-in amplifier(Stanford Research Systems SR830, $V_{\rm ac} = 1$ V, $f \approx 20$ kHz), whose phase sensitive current output is captured on an oscilloscope. As seen in Fig. 4(b), only if some donor $|\uparrow\rangle$ population has been generated by the microwave pulse sequence is a distinct conductivity transient observed during the "readout" pulse—this originates from the Auger electrons produced following laser-induced D^0X generation. The transient decays with a time constant of approximately 40 ms, characteristic of the D^0X excitation rate for our D^0X linewidth (200 MHz) and laser intensity (0.2 mW/mm^2). We maximize the signal by adjusting the lock-in phase and integrate over the first 30 ms of the transient photoconductivity response to produce a unitless measure for the population of the $|\uparrow\rangle$ state, normalizing the result using that measured in the same experiment with a short (10 μs) evolution time.

Figure 4(c) plots this measured $|\uparrow\rangle$ population as a function of free evolution time, 2τ, in the Hahn echo experiment, providing a measure of the electron spin coherence time. Three distinct time scales can be observed in the evolution: for $2\tau \lesssim 1$ ms, the microwave $\pm\pi/2$ pulses consistently project the echo signal into the opposite spin states ($|\uparrow\rangle$ and $|\downarrow\rangle$), as expected, indicating negligible decay in electron spin coherence on this timescale. For 1 ms $\lesssim 2\tau \lesssim 100$ ms the echo signal appears randomly projected between the $|\uparrow\rangle$ and $|\downarrow\rangle$ states, indicating there is a macroscopic coherent state across the electron spin ensemble but its phase varies randomly from one measurement to the next. This "phase-noise" effect is commonly observed in ESR electromagnets for $2\tau \gtrsim 1$ ms and can be attributed to fluctuations of the external magnetic field on a time scale of approximately 1 kHz, which impact the

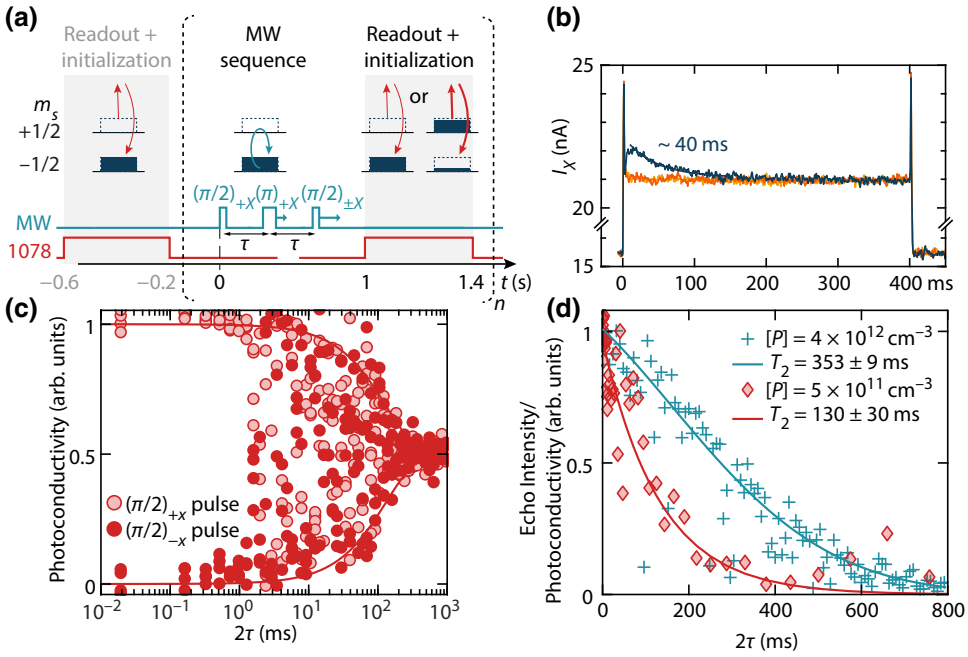

FIG. 4. Pulse sequence and results of the photoconductive coherence time measurement. (a) Applied control sequence, consisting of an initialization laser pulse (also serving as the readout pulse for the previous experiment), the microwave (MW) pulse sequence and the readout laser pulse (also serving as initialization for the next experiment). (b) Photocurrent time trace during the readout laser pulse when applying a single microwave π pulse with (i) B on resonance (dark blue), (ii) B off resonance (orange), and (iii) B on resonance with no microwave pulse (yellow). (c) Two-pulse echo decay measured by integrating a photocurrent during the readout laser pulse as in (b) plotted against the interpulse delay, 2τ (sample [P] $= 5 \times 10^{11}$ cm^{-3} at 4.5 K). (d) Selected (maximum) data points from (c) and accompanying exponential fit to the data indicating $T_2 = 130$ ms. Also shown is the Hahn echo decay measured for [P] $= 4 \times 10^{12}$ cm^{-3} at 1.7 K using a conventional pulsed ESR with only one laser pulse for spin initialization (and not for readout).

net phase acquired by the spin ensemble during an experiment [27]. In a conventional ESR measurement employing detection of both quadrature channels, the effects of such phase noise can be mitigated by recording the magnitude across the two quadrature channels for each experimental shot [27]. In contrast, when using a projective readout method (such as the photoconductivity measurement used here), the effects of phase noise are manifest as random projections into the $|\uparrow\rangle$ and $|\downarrow\rangle$ states, as we observe. Nevertheless, the maximum value of these randomly projected states can, with a sufficient number of measurements, provide a reasonable measure of the overall echo intensity [3]. This phase noise is believed to be limited by the instrumentation and could in principle be improved with superconducting magnets in persistent mode or permanent magnets with magnetic shielding [28]. For $2\tau > 100$ ms the echo intensity collapses due to electron spin decoherence. The timescale of this collapse can be extracted from a fit to the maximum data points [red diamonds in Fig. 4(d)] and we find a coherence time (T_2) of 130 ± 30 ms.

The T_2 we measure above is somewhat shorter than expected for this sample. Instantaneous diffusion is not expected to play a role since the concentration is too low [4,7] ($T_{2,\mathrm{ID}} \approx 5$ s for [P] $= 5 \times 10^{11}$ cm^{-3}). The coherence time is not limited by a T_1 process or by donor-acceptor recombination [23], as an inversion recovery measurement gives a lower bound for such processes as $T_1 > 2$ s. Instead, we expect the intrinsic T_2 to be limited by spectral diffusion from the residual 47 ppm of ^{29}Si nuclear spins at $T_{2,\mathrm{SD}} \approx 0.5$–1 s [29,30]. The apparent discrepancy between this and the measured value is likely due to instrument limitations, in particular sample vibrations within an inhomogeneous magnetic field (caused, for example, by the gas flow in the He cryostat). Indeed, a suggestive "revival" in spin coherence can be observed in the data of [Fig. 4(d)] around 650 ms. While such features are not fully understood, we have observed similar revivals in other measurement when limited by magnetic field noise and believe them to be a consequence of the specific inhomogeneous magnetic field noise spectrum (which varies according to cryostat, sample mount, magnet power supply, etc.). If this interpretation is correct, the coherence time in the sample inferred from the magnitude of the revival would lie in the expected range of 0.5–1 s.

To explore this hypothesis further, we compare the results above with measurements of coherence times observed on a higher doped sample ([P] $= 4 \times 10^{12}$ cm^{-3}) submerged in superfluid helium at 1.7 K, and detected by

conventional ESR combined with optical hyperpolarization via the D^0X transition (using a 200-ms laser pulse). Here, vibrations are significantly reduced and a coherence time of 350 ms is measured [see Fig. 4(d)], consistent with the product of a known instantaneous diffusion term ($T_{2,\mathrm{ID}} = 600$ ms [7]), and a fitted spectral diffusion term $T_{2,\mathrm{SD}} = 530$ ms, in accordance with literature values for the nuclear spin spectral diffusion of 47 ppm ^{29}Si [29,31].

IV. CONCLUSIONS

In summary, we use contactless capacitive measurements to characterize the photoconductivity of doped silicon samples under resonant D^0X excitation. We show how the spin-dependent D^0X photoconductivity can be used as a method to detect pulsed ESR on samples with doping levels below the sensitivity of conventional ESR, with a single-shot signal-to-noise ratio of about 10 for spin ensembles with concentration 5×10^{11} cm^{-3}. However, efforts must be taken to minimize sample vibrations in order to observe coherence times on the timescale of seconds or longer. We find evidence that off-resonant contributions to photoconductivity arise primarily from direct ionization of donors. As a result, this photoconductivity-detected ESR scales down to much smaller ensembles because the ratio of on- to off-resonant photoconductivity, a key factor in the signal-to-noise ratio, would be independent of the donor ensemble size.

ACKNOWLEDGMENTS

The ^{28}Si samples used in this study are prepared from Avo28 crystal produced by the International Avogadro Coordination (IAC) Project (2004-2011) in cooperation among the BIPM, the INRIM (Italy), the IRMM (EU), the NMIA (Australia), the NMIJ (Japan), the NPL (UK), and the PTB (Germany). This research is supported by the Engineering and Physical Sciences Research Council (EPSRC) through UNDEDD (EP/K025945/1) and a Doctoral Training Grant, as well as by the European Unions Horizon 2020 research and innovatioN programme under Grant Agreements No. 688539 (MOS-QUITO) and No. 771493 (LOQO-MOTIONS). The work at Princeton is supported by the NSF MRSEC Program (Grant No. DMR-1420541) and the ARO (Grant No. W911NF-13-1-0179).

APPENDIX: ELECTRON CARRIER GENERATION RATES UNDER ILLUMINATION

The on-resonance carrier generation rate $G_{D^0\mathrm{X}}$ can be calculated from the Einstein coefficient B^f_{12} (related to the oscillator strength [16]) of the D^0X transition and its measured lineshape function $g(f, f_0)$ as

$$G_{D^0\mathrm{X}} = N^0 B^f_{12} \int_0^\infty g(f, f_0)\rho(f)df\,. \tag{A1}$$

Here N^0 is the density of neutral donors and $\rho(f) = I_L/(c/n_{\mathrm{Si}})\delta(f_0)$ is the δ-like power spectral density of the laser within the silicon sample due to a laser with intensity I_L. The linewidth of the laser is much smaller than the D^0X linewidth Δf, and hence the integral yields

$$G_{D^0\mathrm{X}} = N^0 B^f_{12} \frac{I_L}{c/n_{\mathrm{Si}}} \frac{2}{\pi\,\Delta f}. \tag{A2}$$

The carrier generation rate due to resonant bound-exciton generation is thus proportional to the laser intensity, the donor density and inversely proportional to the D^0X linewidth. $B_{12} = 3.1 \times 10^{16}$ J^{-1} m^3 s^{-2} for P and c/n_{Si} is the speed of light in silicon $= 8.1 \times 10^7$ ms^{-1}.

Off resonance, the direct ionization rate of the laser—assumed to be the main cause of extrinsic photoconductivity—scales with the capture cross section $\sigma_{N^0\to N^+}$ according to [33]

$$G_{\mathrm{direct}} = N^0 \frac{I_L}{\hbar\omega}\sigma_{N^0\to N^+}. \tag{A3}$$

Data for $\sigma_{N^0\to N^+}$ of phosphorus at a wavelength of 1078 nm are scarce, but can be extrapolated from the figures presented in Ref. [22]. By comparing the two equations, it can be observed that the ratio of on- to off-resonant excitation is independent of donor density and laser intensity.

Finally, we present a few remarks regarding the band-to-band excitation of electrons from the valence band into the conduction band. As discussed in the main text, the required phonon absorption is heavily surpressed due to the low temperature and hence very small absorption coefficients are measured for silicon below the bandgap and at low temperatures [25]. Data close to the bandgap are scarce but unpublished measurements of R. Nawrodt (Friedrich Schiller University Jena) give an upper limit for the intrinsic absorption of $\alpha_{\mathrm{Si}}(3\ \mathrm{K}, 1.15\ \mathrm{eV}) \approx 3 \times 10^{-4}$ cm^{-1}, although the exact origin of the absorption for this wavelength remains unclear and could still be of extrinsic origin. Still, the carrier generation rate associated with this upper limit for intrinsic absorption is much smaller than the expected G_{direct} at the donor densities studied here. We thus do not expect intrinsic absorption to contribute to the photoconductivities presented in this paper.

[1] P. Becker, H. J. Pohl, H. Riemann, and N. Abrosimov, Enrichment of silicon for a better kilogram, Phys. Status Solidi (a) **207**, 49 (2010).

[2] M. Steger, K. Saeedi, M. L. W. Thewalt, J. J. L. Morton, H. Riemann, N. V. Abrosimov, P. Becker, and H.-J. Pohl, Quantum information storage for over 180 s using donor spins in a 28Si "semiconductor vacuum", Science **336**, 6086 (2012).

[3] K. Saeedi, S. Simmons, J. Z. Salvail, P. Dluhy, H. Riemann, N. V. Abrosimov, P. Becker, H.-J. Pohl, J. J. L. Morton, and

M. L. W. Thewalt, Room-temperature quantum bit storage exceeding 39 minutes using ionized donors in silicon-28, Science **342**, 830 (2013).

[4] A. M. Tyryshkin, S. Tojo, J. J. L. Morton, H. Riemann, N. V. Abrosimov, P. Becker, H.-J. Pohl, T. Schenkel, M. L. W. Thewalt, K. M. Itoh, and S. A. Lyon, Electron spin coherence exceeding seconds in high-purity silicon, Nat. Mater. **11**, 143 (2012).

[5] Gary Wolfowicz, Alexei M. Tyryshkin, Richard E. George, Helge Riemann, Nikolai V. Abrosimov, Peter Becker, Hans-Joachim Pohl, Mike L. W. Thewalt, Stephena Lyon, and John J. L. Morton, Atomic clock transitions in silicon-based spin qubits, Nat. Nanotechnol. **8**, 561 (2013).

[6] Juha T. Muhonen, Juan P. Dehollain, Arne Laucht, Fay E. Hudson, Rachpon Kalra, Takeharu Sekiguchi, Kohei M. Itoh, David N. Jamieson, Jeffrey C. McCallum, Andrew S. Dzurak, and Andrea Morello, Storing quantum information for 30 seconds in a nanoelectronic device, Nat. Nanotechnol. **9**, 986 (2014).

[7] Vadim V. Kurshev and Tsuneki Ichikawa, Effect of spin flip-flop on electron-spin-echo decay due to instantaneous diffusion, J. Magn. Res. (1969) **96**, 563 (1992).

[8] Arthur Schweiger and Gunnar Jeschke, *Principles of Pulse Electron Paramagnetic Resonance* (Oxford University Press, Oxford, UK, 2001).

[9] Andre R. Stegner, Christoph Boehme, Hans Huebl, Martin Stutzmann, Klaus Lips, and Martin S. Brandt, Electrical detection of coherent ^{31}P spin quantum states, Nat. Phys. **2**, 835 (2006).

[10] D. R. McCamey, H. Huebl, M. S. Brandt, W. D. Hutchison, J. C. McCallum, R. G. Clark, and A. R. Hamilton, Electrically detected magnetic resonance in ion-implanted Si:P nanostructures, Appl. Phys. Lett. **89**, 182115 (2006).

[11] S.-Y. Paik, S.-Y. Lee, W. J. Baker, D. R. McCamey, and C. Boehme, T_1 and T_2 spin relaxation time limitations of phosphorous donor electrons near crystalline silicon to silicon dioxide interface defects, Phys. Rev. B **81**, 075214 (2010).

[12] C. C. Lo, M. Urdampilleta, P. Ross, M. F. Gonzalez-Zalba, J. Mansir, S. A. Lyon, M. L. W. Thewalt, and J. J. L. Morton, Hybrid optical–electrical detection of donor electron spins with bound excitons in silicon, Nat. Mater. **14**, 490 (2015).

[13] A. Yang, M. Steger, H. J. Lian, M. L. W. Thewalt, M. Uemura, A. Sagara, K. M. Itoh, E. E. Haller, J. W. Ager, S. A. Lyon, M. Konuma, and M. Cardona, High-resolution photoluminescence measurement of the isotopic-mass dependence of the lattice parameter of silicon, Phys. Rev. B **77**, 113203 (2008).

[14] David P. Franke, Michael Szech, Florian M. Hrubesch, Helge Riemann, Nikolai V. Abrosimov, Peter Becker, Hans-Joachim Pohl, Kohei M. Itoh, Michael L. W. Thewalt, and Martin S. Brandt, Electron nuclear double resonance with donor-bound excitons in silicon, Phys. Rev. B **94**, 235201 (2016).

[15] Gary Wolfowicz, Matias Urdampilleta, Mike L. W. Thewalt, Helge Riemann, Nikolai V. Abrosimov, Peter Becker, Hans-Joachim Pohl, and John J. L. Morton, Conditional Control of Donor Nuclear Spins in Silicon Using Stark Shifts, Phys. Rev. Lett. **113**, 157601 (2014).

[16] W. Schmid, Auger lifetimes for excitons bound to neutral donors and acceptors in Si, Phys. Status Solidi (b) **84**, 529 (1977).

[17] Jerzy Krupka, Jonathan Breeze, Anthony Centeno, Neil Alford, Thomas Claussen, and Leif Jensen, Measurements of permittivity, dielectric loss tangent, and resistivity of float-zone silicon at microwave frequencies, IEEE Trans. Microwave Theory Techniques **54**, 3995 (2006).

[18] The polarizability and concentration of phosphorus is negligible compared to the polarizability of the silicon lattice [32].

[19] P. J. Dean, W. F. Flood, and G. Kaminsky, Absorption due to bound excitons in silicon, Phys. Rev. **163**, 721 (1967).

[20] P. Norton, T. Braggins, and H. Levinstein, Impurity and lattice scattering parameters as determined from Hall and mobility analysis in n-type silicon, Phys. Rev. B **8**, 5632 (1973).

[21] N. Sclar, Properties of doped silicon and germanium infrared detectors, Prog. Quantum Electron. **9**, 149 (1984).

[22] N. Sclar, Asymmetries in photoconductive properties of donor and acceptor impurities in silicon, J. Appl. Phys. **55**, 2972 (1984).

[23] P. Dirksen, A. Henstra, and W. Th. Wenckebach, An electron spin echo study of donor-acceptor recombination, J. Phys.: Condens. Matter **1**, 7085 (1989).

[24] M. Cardona, T. Meyer, and M. L. W. Thewalt, Temperature Dependence of the Energy Gap of Semiconductors in the Low-temperature Limit, Phys. Rev. Lett. **92**, 196403 (2004).

[25] G. G. Macfarlane, T. P. McLean, J. E. Quarrington, and V. Roberts, Fine structure in the absorption-edge spectrum of Si, Phys. Rev. **111**, 1245 (1958).

[26] K. Rajkanan, R. Singh, and J. Shewchun, Absorption coefficient of silicon for solar cell calculations, Solid State Electron. **22**, 793 (1979).

[27] A. M. Tyryshkin, J. J. L. Morton, S. C. Benjamin, A. Ardavan, G. A. D. Briggs, J. W. Ager, and S. A. Lyon, Coherence of spin qubits in silicon, J. Phys. Condens. Mater. **18**, S783 (2006).

[28] T. Ruster, C. T. Schmiegelow, H. Kaufmann, C. Warschburger, F. Schmidt-Kaler, and U. G. Poschinger, A long-lived Zeeman trapped-ion qubit, Appl. Phys. B: Lasers Opt. **122**, 254 (2016).

[29] E. Abe, A. M. Tyryshkin, S. Tojo, J. J. L. Morton, W. M. Witzel, A. Fujimoto, J. W. Ager, E. E. Haller, J. Isoya, S. A. Lyon, M. L. W. Thewalt, and K. M. Itoh, Electron spin coherence of phosphorus donors in silicon: Effect of environmental nuclei, Phys. Rev. B - Condens. Matter Mater. Phys. **82**, 9 (2010).

[30] Wayne M. Witzel, Malcolm S. Carroll, Andrea Morello, Łukasz Cywiński, and S. Das Sarma, Electron Spin Decoherence in Isotope-Enriched Silicon, Phys. Rev. Lett. **105**, 187602 (2010).

[31] Another difference between the two T_2 measurements is the delay time between the end of the polarizing laser pulse and beginning of the Hahn echo sequence (900 ms for the echo-detected experiments and 200–450 ms for the photoconductivity-detected ESR experiments).

Charge reconfiguration and resulting Stark-field noise during the dark period could induce decoherence, however, while these effects have not been studied systematically, no difference in photoconductivity-measured T_2 has been observed for the two delay times 200 ms and 450 ms.

[32] S. Dhar and Alan H. Marshak, Static dielectric constant of heavily doped semiconductors, Solid State Electron. **28**, 763 (1985).

[33] Richard H. Bube, *Photoelectronic Properties of Semiconductors* (Cambridge University Press, Cambridge, UK, 1992).